RSC Advances

PAPER

View Article Online
View Journal | View Issue

Cite this: *RSC Adv.*, 2017, **7**, 8491

Tuning the solid-state fluorescence of chalcone crystals *via* molecular coplanarity and J-aggregate formation†

Fangfang Yu,[a] Mingliang Wang,*[a] Hao Sun,[a] Yaqi Shan,[a] Man Du,[a] Arshad Khan,[a] Rabia Usman,[a] Wei Zhang,[a] Hongbin Shan[a] and Chunxiang Xu*[b]

Received 28th November 2016
Accepted 18th January 2017

DOI: 10.1039/c6ra27458g

www.rsc.org/advances

Four chalcones bearing the 1,3-diarylpropenone moiety 3-(9-anthryl)-1-(4-chloro)prop-2-en-1-one (**I**), 3-(1-pyrenyl)-1-(4-chlorophenyl)prop-2-en-1-one (**II**), 1-phenyl-3-(1-pyrenyl)prop-2-en-1-one (**III**) and 3-(1-pyrenyl)-1-(4-nitrophenyl)prop-2-en-1-one (**IV**) were synthesized and different crystal forms were obtained from different solvents by slow evaporation including **I** (I_a, I_b), **II** (II_a, II_b, II_c), **III** (III_a, III_b, III_c, III_d) and **IV** (IV_a, IV_b). Their structures and optical properties were characterized by single crystal X-ray diffraction (SCXRD), powder X-ray diffraction (PXRD), thermogravimetric analysis (TGA) and differential scanning calorimetry (DSC), UV-Vis absorption spectroscopy and fluorescence spectroscopy. Hirshfeld surface calculations were also used for intermolecular interaction analysis. It has been found that polymorphism and conformational isomorphism exist in these crystals. I_b and III_a adopt a *cis* configuration with respect to the central C=C bond while the other forms exhibit a *trans* configuration, except for those without single crystal X-ray analysis. Both I_b and II_b have two crystallographically independent molecules in their asymmetrical unit which has not been found in reported chalcone crystals. Those crystals with a *cis* configuration show a higher melting point and no fluorescence. Crystals with a *trans* configuration are fluorescent and their emission wavelengths are mainly effected by the torsion extent of the molecules and J-aggregate formation.

Introduction

Crystal polymorphism, a phenomenon having been concentrated on for years, is generally defined as the possibility of the same compound existing in more than one crystalline modification in the solid state.[1,2] Polymorphs differ in a number of significant properties such as solubility, stability and bioavailability[3–5] that catering for a series of potential applications in pharmaceuticals,[6] pigments,[7] explosives[8] and so on. What's more, it is an ideal approach to compare different polymorphs for the purpose of deeply elucidating the relationships between the solid state properties and crystal structures based on the same molecules.[9,10] Molecules with conformational flexibility usually show a larger extent of freedom than rigid ones so that a wide range of polymorphism might be obtained from them.[11–13] Current research on the solid state fluorescence of polymorphism indicate that stacking geometries of molecules and intermolecular electronic interactions in the solid state have a significant influence on fluorescent properties of organic luminescent polymorphs.[14–17] And many studies on luminescence properties suggest that J-aggregate formation is beneficial to fluorescence emission.[18,19]

Chalcone, the important class of compound bearing α,β-unsaturated ketone moiety, increasingly attracts more attention from academic circles and pharmaceutical industry. Chalcones are found to have many applications because of their properties such as bioactivities,[5] optical properties[20,21] and photochemical characteristics[20,22] all of which are researched and applied widespread. Furthermore, chalcones are intermediates of many heterocyclic compounds such as pyrazole, quinoline, pyrimidine and so on.[23] In the phenomenon of *cis–trans* configuration, *trans* configuration exhibits greater stability than *cis* which is suggested by easier formation of *trans* configuration and the approach of quantum chemistry also gave explanation to

[a]*School of Chemistry and Chemical Engineering, Southeast University, Nanjing 211189, P. R. China. E-mail: wangmlchem@seu.edu.cn; Tel: +86 2585092237*

[b]*State Key Laboratory of Bioelectronics, Southeast University, Nanjing 210096, P. R. China. E-mail: xcxseu@seu.edu.cn*

† Electronic supplementary information (ESI) available: Microscopy graphs of all forms; NMR spectra of chalcone compounds; comparing of PXRD experimental patterns (black) of crystals with simulated patterns (red); absorption spectra of crystals in acetonitrile solvent; fluorescence spectra (λ_{ex} = 365 nm) in cyclohexane solution for all forms; IR spectra of crystals; Hirshfeld surface mapped with d_{norm} and fingerprint plots of crystals; solvents for crystal preparation; melting point, enthalpy and decomposition temperature range of all crystals; the maximum absorption and emission peak of all solids; contributions of individual intermolecular interactions to the Hirshfeld surface of all crystals; X-ray crystallographic information files (CIF) for eight crystals. CCDC 1473276, 1473277, 1473283, 1473284, 1477084, 1473288, 1473285 and 1473292. For ESI and crystallographic data in CIF or other electronic format see DOI: 10.1039/c6ra27458g

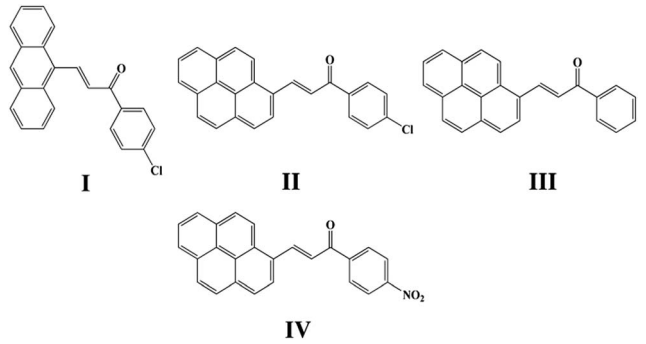

Scheme 1 Chemical structure of I, II, III, IV.

stability difference.[24,25] Thus a number of crystals of chalcone have been reported while crystals with *cis* configuration are hardly to find for its strikingly steric effect. In our former research done by Zhang Ruimin *et al.*,[17] several chalcone polymorphs which show *cis* or *trans* configuration have been investigated. In this research, four new chalcones were synthesized (Scheme 1), while the polymorphism being found in this research is conformational and configurational isomorphism. Furthermore, conformational isomorphism is rarely reported for the compound of chalcone, especially when referring it to two conformers in crystal asymmetry unit.

Fluorescent properties of chalcone polymorphism in the solid state can be rarely to found in literatures reported before. Previously, we readily prepared several high quality chalcone polymorphs and π-stacked geometries plays a key role in fluorescent properties of chalcone polymorphism.[17] Therefore, we deduce that there can be some other factors related to optical properties of chalcone and we investigated in different chalcone polymorphs to find that molecular planarity and aggregation exert great influence on fluorescent properties of chalcone polymorphism in the solid state, which may offer a significant direction in application of organic light-emitting materials.[26]

Experimental section

Materials synthesis

As shown in Scheme 2, a mixture of 4-chloroacetophenone (1.54 g), 9-anthrylaldehyde (2.3 g) and 3 M of aqueous sodium hydroxide (6 mL) in ethanol (20 mL) was stirred at room temperature for 3 h. The crude product was collected by filtration and recrystallized from ethyl acetate/acetic acid (v/v = 1 : 1) resulting in orange crystals as 3-(9-anthryl)-1-(4-chloro)prop-2-en-1-one (**I**): yield: 80%, mp: 136–138 °C. ^{1}H NMR ($CDCl_3$, Fig. 2S, ESI†): δ (ppm) 8.81 (d, 1H), 8.49 (s, 1H), 8.36–8.19 (m, 2H), 8.04 (dd, 4H), 7.63–7.46 (m, 7H). ^{13}C NMR ($CDCl_3$, Fig. 3S, ESI†): δ (ppm) 188.36, 142.47, 139.59, 136.22, 131.32, 130.48, 130.12, 129.92, 129.66, 129.11, 128.98, 128.64, 126.55, 125.48, 125.20.

As can be seen from Scheme 2, a mixture of acetophenone (1.2 g), 1-pyrenecarboxaldehyde (2.3 g) and 3 M of aqueous sodium hydroxide (6 mL) in ethanol (20 mL) was stirred at room temperature for 3 h. The resulting solid was collected by filtration and recrystallized from ethyl acetate/acetic acid (v/v = 1 : 1) to get orange crystals as 1-phenyl-3-(1-pyrenyl)prop-2-en-1-one (**III**): yield: 70%, mp: 163–165 °C. ^{1}H NMR ($CDCl_3$, Fig. 4S, ESI†): δ (ppm) 8.82 (d, 1H), 8.31 (d, 1H), 8.17 (d, 1H), 8.06 (dd, 4H), 8.00–7.80 (m, 5H), 7.65 (d, 1H), 7.61–7.42 (m, 3H). ^{13}C NMR ($CDCl_3$, Fig. 5S, ESI†): δ (ppm) 189.67, 140.85, 137.96, 132.40, 132.36, 130.71, 130.11, 129.75, 128.27, 128.16, 128.10, 127.99, 126.78, 125.76, 125.54, 125.40, 124.46, 124.31, 123.97, 123.52, 123.08, 121.92. Similarly, 3-(1-pyrenyl)-1-(4-chlorophenyl)prop-2-en-1-one (**II**) and 3-(1-pyrenyl)-1-(4-nitrophenyl)prop-2-en-1-one (**IV**) were synthesized according to the procedure with 4-chloroacetophenone and 4-nitroacetophenone as starting material respectively. 1-3-(1-Pyrenyl)-1-(4-chlorophenyl) prop-2-en-1-one (**II**): ^{1}H NMR ($CDCl_3$, Fig. 6S, ESI†): δ (ppm) 8.88 (d, 1H), 8.40 (d, 1H), 8.26 (d, 1H), 8.14 (d, 2H), 8.09–8.01 (m, 3H), 8.01–7.93 (m, 4H), 7.63 (d, 1H), 7.45 (d, 2H). ^{13}C NMR ($CDCl_3$, Fig. 7S, ESI†): δ (ppm) 188.63, 141.73, 139.17, 136.60, 132.98, 131.18, 130.58, 130.32, 129.89, 128.92, 128.76, 128.70, 128.30, 127.32, 127.21, 126.26, 126.08, 125.92, 124.92, 124.83, 124.44, 124.00, 122.95, 122.33. 3-(1-Pyrenyl)-1-(4-nitrophenyl) prop-2-en-1-one (**IV**): ^{1}H NMR ($CDCl_3$, Fig. 8S, ESI†): δ (ppm) 9.05 (d, 1H), 8.54 (d, 1H), 8.44 (d, 1H), 8.41–8.33 (m, 2H), 8.33–8.19 (m, 6H), 8.17 (d, 1H), 8.14–8.01 (m, 2H), 7.77 (d, 1H). ^{13}C NMR ($CDCl_3$, Fig. 9S, ESI†): δ (ppm) 188.59, 143.30, 133.52, 131.31, 130.77, 130.68, 129.46, 129.23, 129.17, 127.98, 127.34, 126.52, 126.43, 126.25, 125.14, 125.05, 124.56, 124.24, 123.92, 122.80, 122.31.

$\mathbf{I_a}$ was recrystallized in ethyl acetate/acetic acid (v/v = 1 : 1) as orange rod like crystal. $\mathbf{I_b}$ was obtained from ethanol in which $\mathbf{I_a}$ was dissolved. Slow evaporation of the solvent at room temperature for 4–5 days yielded yellow rod like crystal.

$\mathbf{II_a}$ was recrystallized in ethyl acetate/acetic acid (v/v = 1 : 1) mixed solvents as orange-red plate crystal. $\mathbf{II_b}$ was obtained from ethyl acetate/dichloromethane (v/v = 1 : 1) mixed solvents in which $\mathbf{II_a}$ was dissolved. Slow evaporation of the solvents at room temperature for 2–3 days yielded orange rod like crystal. $\mathbf{II_c}$ was obtained from isopropanol in which $\mathbf{II_a}$ was dissolved. Slow evaporation at room temperature for 2–3 days yielded small yellow plate crystal.

$\mathbf{III_a}$ was obtained from mixed solvent of ethanol/ethyl acetate (v/v = 1 : 1) with $\mathbf{III_a}$ dissolved in it. Slow evaporation of the solvents at room temperature for 4–5 days yielded a yellow transparent crystal. $\mathbf{III_b}$ was gained from acetonitrile or ethanol/ethyl acetate (v/v = 1 : 1) mixed solvents in which $\mathbf{III_a}$ was dissolved. Slow evaporation of the solvents at room temperature for 4–5 days yielded red transparent plate crystal. $\mathbf{III_c}$ was recrystallized in acetonitrile/chloroform (v/v = 1) or acetic acid/ethyl acetate (v/v = 1 : 1) mixed solvent as orange needle like crystal. $\mathbf{III_d}$ was recrystallized after 3–4 days' slow evaporation at room temperature with $\mathbf{III_a}$ dissolved in isopropanol as yellow plate crystal.

$\mathbf{IV_a}$ was obtained from acetonitrile/dichloromethane (v/v = 1 : 1) mixed solvents with 2–3 days slow evaporation at room temperature yielding red needle like crystal. $\mathbf{IV_b}$ was recrystallized in acetonitrile/dichloromethane (v/v = 1 : 1) mixed solvents as a purple crystal after 2–3 days slow evaporation at room temperature.

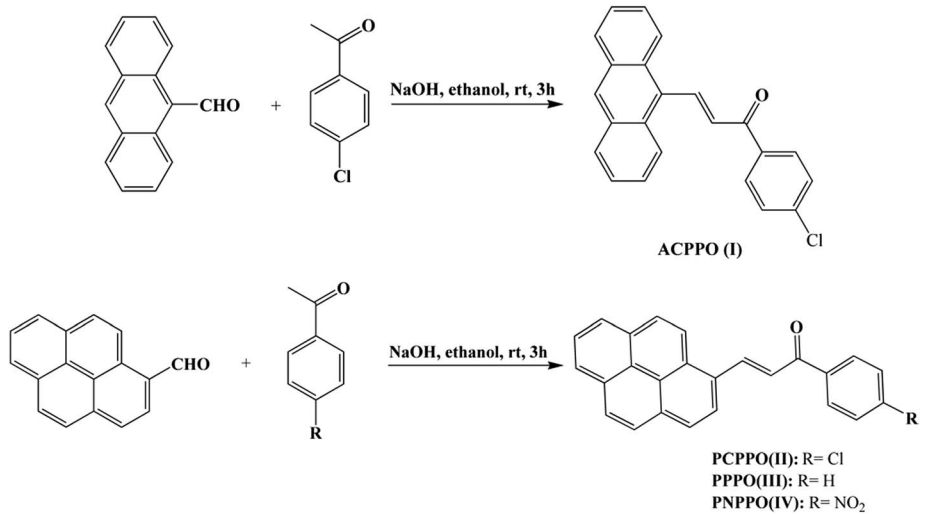

Scheme 2 Preparation of chalcone I, II, III, IV.

Characterization methods

NMR analysis. ^{1}H NMR and ^{13}C NMR spectra were recorded at 303 K on a Bruker Avance 500 MHz NMR spectrometer using $CDCl_3$ as a solvent and TMS as an internal standard.

X-ray diffraction. The PXRD patterns for the eleven crystals were recorded using a 18 kW advance X-ray diffractometer with Cu K α radiation (λ = 1.54056 Å). Single X-ray diffraction data for these crystals were collected on Nonius CAD4 diffractometer with Mo Kα radiation (λ = 0.71073 Å). The structures were solved with direct methods using the SHELXS-2014 program and refined anisotropically using full-matrix least-squares procedure.

Spectroscopic measurements. UV-Vis absorption spectra were recorded on a Shimadzu UV-2600 spectrometer. Fluorescence spectra were obtained on a Horiba FluoroMax 4 spectrofluorometer. Infrared spectra were collected on a Bruker Tensor 27 FT-IR spectrometer.

Fluorescence microscopy images. Fluorescence microscopy images were obtained on an Olympus BX51 imaging system excited at 365 nm.

Thermogravimetric analysis (TGA) and differential scanning calorimetry (DSC). TGA/DSC patterns were recorded with a Mettler-Toledo TGA/DSC Thermogravimetric Analyzer with the temperature scanned from 50 to 550 °C at 10 °C min^{-1}.

Hot stage microscopy (HSM). Hot stage microscopy was performed on a LEICA DM750P microscope using a Mettler-Toledo FP82HT hot stage. The data were visualized using the AMC Capture software.

Results and discussion

Crystal structure

Despite considerable experimental endeavor, attempts to grow single crystals of **II** in isopropanol ($\mathbf{II_c}$), **III** in isopropanol ($\mathbf{III_d}$) and **IV** in acetonitrile/dichloromethane (v/v = 1 : 1) ($\mathbf{IV_b}$) were unsuccessful. Thus, single crystal X-ray diffraction (SCXRD) analysis was performed for all other forms showing independent framework arrangements and cell parameters (Table 1). Additionally SCXRD of $\mathbf{III_c}$ was reported.[27]

Crystal $\mathbf{I_a}$ crystallizes in monoclinic system with space group of $P2_1/c$ while $\mathbf{I_b}$ crystallizes in orthorhombic system with space group of $Pca2_1$. $\mathbf{I_a}$ shows *trans* configuration while $\mathbf{I_b}$ exhibits *cis* configuration (Fig. 1a and 2a). $\mathbf{I_a}$ is connected by weak hydrogen bond (Table 2) (O···H16A distance: 2.46 Å; C–O···H angle: 161°) and C(alkene)–H···π (6 atoms of anthracene) (Table 3) interactions on ac plane (Fig. 1b). $\mathbf{I_b}$ possesses two types of molecules in its crystal structure (Fig. 2a). Molecules A are linked by weak hydrogen bonds (Table 2) (O1A···H16A distance: 2.54 Å; C–O···H angle: 164°) and C(alkene)–H···π (6 atoms of anthracene) (Table 3) interactions on ac plane (Fig. 2b). Likewise, weak hydrogen bonds (Table 2) (O2B···H16B distance: 2.56 Å; C–O···H angle: 159°) and C(alkene)–H···π (6 atoms of anthracene) (Table 3 and Fig. 2b) connect between molecules B on ac plane. Besides, molecules A and B are separately linked by C(anthracene)–H···π (benzene ring) (Table 3 and Fig. 2c) along *b* axis.

Crystal $\mathbf{II_a}$ crystallizes in monoclinic system with space group $C2/c$ while $\mathbf{II_b}$ crystallizes in orthorhombic system with space group $P2_12_12_1$. Both $\mathbf{II_a}$ and $\mathbf{II_b}$ show *trans* configuration. It is evident that molecules in the structure of $\mathbf{II_a}$ are connected by C–O···π (6 atoms of pyrene ring), C–H···π (6 atoms of pyrene ring) and C–H···π (benzene ring) interactions on ac plane (Table 3 and Fig. 3b). Molecules in $\mathbf{II_b}$ are linked through interactions of C–Cl···π (6 atoms of pyrene ring) and C–Cl···π (benzene ring) along *c* axis (Fig. 4b).

$\mathbf{III_a}$ crystallizes in triclinic system with space group $P\bar{1}$ and it shows *cis* configuration. Both $\mathbf{III_b}$ and $\mathbf{III_c}$ crystallizes in monoclinic system while their space groups are $P2/c$ and $P2_1$ respectively. Besides, they all show *trans* configuration. As shown in Fig. 5b, molecules are packing along a axis through C–H···O (O···H8A distance: 2.43 Å; C–O···H angle: 138°) (Table 2) and C(pyrene)–O···π (benzene ring) (Table 3) interactions in $\mathbf{III_a}$. In Fig. 6a, it can be seen that $\mathbf{III_b}$ owns two types of

Table 1 Crystal data and structure refinement

Crystal	$\mathbf{I_a}$	$\mathbf{I_b}$	$\mathbf{II_a}$	$\mathbf{II_b}$
Formula	$C_{23}H_{15}ClO$	$C_{46}H_{30}Cl_2O_2$	$C_{25}H_{15}ClO$	$C_{25}H_{15}ClO$
Temperature/K	293	293	293	293
Crystal size/mm^3	0.30 × 0.10 × 0.10	0.20 × 0.10 × 0.10	0.20 × 0.20 × 0.10	0.20 × 0.10 × 0.10
Morphology	Rod like	Rod like	Plate	Rod like
Melting point/°C	128	129	135	140
Configuration	*trans*	*cis*	*trans*	*trans*
Crystal system	Monoclinic	Orthorhombic	Monoclinic	Orthorhombic
Space group	$P2_1/c$	$Pca2_1$	$C2/c$	$P2_12_12_1$
a/Å	5.4320(11)	10.831(2)	30.665(6)	31.234(6)
b/Å	19.431(4)	10.431(2)	5.5070(11)	4.8180(10)
c/Å	16.208(3)	30.703(6)	21.295(4)	11.669(2)
α/°	90.00	90.00	90.00	90.00
β/°	95.65(3)	90.00	92.38(3)	90.00
γ/°	90.00	90.00	90.00	90.00
V/Å^3	1702.4(6)	3468.8(12)	3593.0(12)	1756.0(6)
Z	4	4	8	4
ρ (calcd)/Mg m^{-3}	1.337	1.313	1.356	1.388
θ range for data collection/°	1.641–25.375	1.326–25.373	1.329–25.400	1.304–25.370
F(000)	712	1424	1520	760
R_1, wR_2 ($I > 2\sigma(I)$)	0.0841, 0.1314	0.0551, 0.0969	0.0986, 0.2173	0.0710, 0.0861
R_1, wR_2 (all data)	0.1980, 0.1644	0.1141, 0.1132	0.2216, 0.2764	0.1937, 0.1172
Goodness-of-fit	1.001	0.998	1.002	1.004
CCDC	1473276	1473277	1473283	1473284

Crystal	$\mathbf{III_a}$	$\mathbf{III_b}$	$\mathbf{III_c}$	$\mathbf{IV_a}$
Formula	$C_{25}H_{16}O$	$C_{50}H_{32}O_2$	$C_{25}H_{16}O$	$C_{25}H_{15}NO_3$
Temperature/K	293	293	293	293
Crystal size/mm^3	0.20 × 0.20 × 0.10	0.30 × 0.20 × 0.10	0.20 × 0.10 × 0.10	0.20 × 0.10 × 0.10
Morphology	Plate	Plate	Needle like	Needle like
Melting point/°C	122	162	144	215
Configuration	*cis*	*trans*	*trans*	*trans*
Crystal system	Triclinic	Monoclinic	Monoclinic	Monoclinic
Space group	$P\bar{1}$	$P2/c$	$P2_1$	$P2_1/n$
a/Å	5.5050(11)	28.811(6)	4.6720(9)	7.3870(15)
b/Å	9.6100(19)	5.4880(11)	22.405(5)	7.8470(16)
c/Å	16.517(3)	21.784(4)	8.2100(16)	32.089(6)
α/°	99.15(3)	90.00	90.00	90.00
β/°	98.70(3)	100.25(3)	106.02(3)	94.00(3)
γ/°	100.80(3)	90.00	90.00	90.00
V/Å^3	832.5(3)	3389.4(12)	826.0(3)	1855.5(7)
Z	2	4	2	4
ρ (calcd)/Mg m^{-3}	1.326	1.303	1.336	1.351
θ range for data collection/°	1.271–25.369	1.436–25.357	1.818–25.397	2.545–25.364
F(000)	348	1392	348	784
R_1, wR_2 ($I > 2\sigma(I)$)	0.0960, 0.1651	0.0693, 0.1072	0.0569, 0.1087	0.0777, 0.1285
R_1, wR_2 (all data)	0.2175, 0.2068	0.1715, 0.1313	0.1169, 0.1284	0.2004, 0.1651
Goodness-of-fit	1.002	1.001	1.002	1.000
CCDC	1477084	1473288	1473285	1473292

molecules in its asymmetry unit and both of them are connected by C–H···π and C–O···π interactions on ac plane. In detail, C–H···π (6 atoms of pyrene ring) and C–O···π (6 atoms of pyrene ring) (Table 3) link between neighboring type A molecules while type B molecules are only connected through C–H···π (6 atoms of pyrene ring) (Table 3). And in Fig. 7b, molecules in $\mathbf{III_c}$ are packing on ab plane with slipped face-to-face π···π interaction.

$\mathbf{IV_a}$ crystallizes in monoclinic system with space group $P2_1/n$ and it exhibits *trans* configuration. As shown in Fig. 8b, molecules are stacking along b axis with weak hydrogen bond C–H···O (O···H7A distance: 2.55 Å; C–O···H angle: 141°) (Table 2), C(alkene)–O···π (6 atoms of pyrene ring) and N–O···π (6 atoms of pyrene ring) (Table 3) interactions on *ac* plane.

In a word, $\mathbf{I_a}$, $\mathbf{II_a}$, $\mathbf{II_b}$, $\mathbf{III_b}$, $\mathbf{III_c}$, $\mathbf{IV_a}$ adopt *trans* configuration while $\mathbf{I_b}$ and $\mathbf{III_a}$ adopt *cis* configuration with respect to the central C=C bond. Thus, chalcones **I** and **III** exist

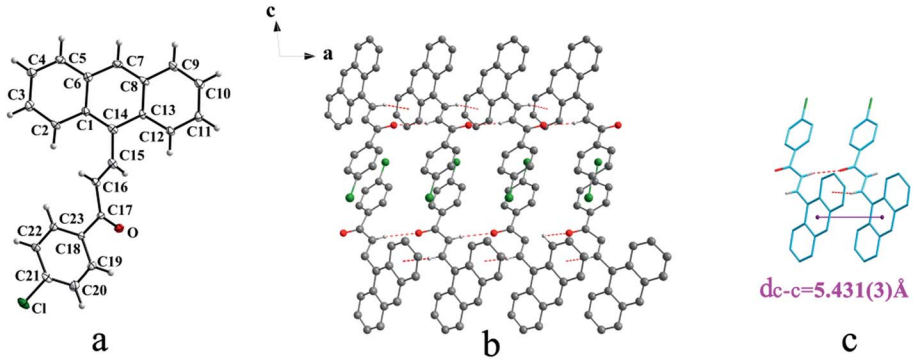

Fig. 1 Structure of form I_a: (a) *trans* configuration, (b) molecules are linked by hydrogen bonds and C–H···π interactions on ac plane, (c) molecules are stacking along *a* axis with hydrogen bonds and C–H···π interactions. The violet line represents the closest centroid distance (d_{c-c} = 5.431(3) Å) between the adjacent anthracene rings. The dotted lines show hydrogen bonds and C–H···π interactions, respectively. Hydrogen atoms not participating in the interactions have been omitted for clarity.

configurational isomers while $\mathbf{II_a}$, $\mathbf{II_b}$ and $\mathbf{III_b}$, $\mathbf{III_c}$ are conformational isomers in the solid state. Furthermore, $\mathbf{I_b}$ and $\mathbf{III_b}$ have two distinct molecules with different conformation in the unit cell. Besides, it can be found that all crystal forms mentioned above adopt parallel face-to-face slipped stacked arrangement for anthracene or pyrene chromophores. According to exciton coupling theory, J-aggregates ($0 < \alpha \leq 54.7°$) exhibit red shifted bands (α is the aligned angle is between transitional moments and the center-to-center axis of the two

Table 2 Intermolecular hydrogen bonds parameters

Crystal	Interaction	D–H (Å)	H···A (Å)	D···A (Å)	∠D–H···A (°)
$\mathbf{I_a}$	C_{16}–$H_{(16A)}$···O	0.93	2.46	3.357(6)	161
$\mathbf{I_b}$	C_{16A}–$H_{(16A)}$···$O_{(1A)}$	0.93	2.54	3.445(8)	164
	C_{16B}–$H_{(16B)}$···$O_{(2B)}$	0.93	2.56	3.442(8)	159
$\mathbf{III_a}$	C_8–$H_{(8A)}$···O	0.93	2.43	3.182(7)	138
$\mathbf{IV_a}$	C_7–$H_{(7A)}$···$O_{(1)}$	0.93	2.55	3.325(5)	141

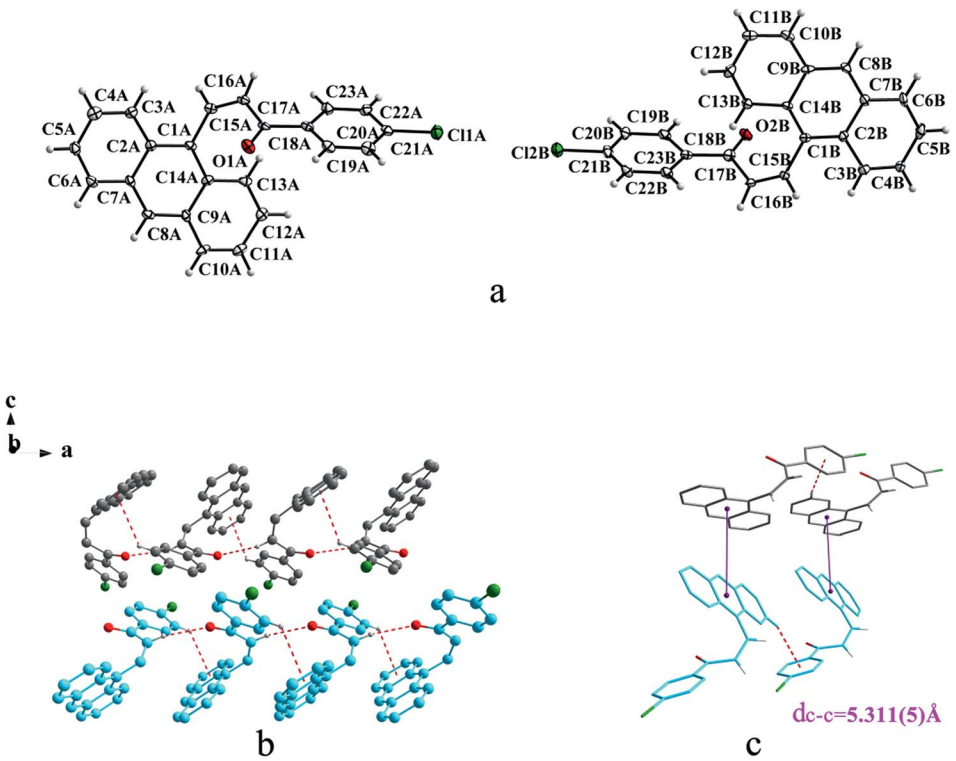

Fig. 2 Structure of form I_b: (a) *cis* configuration, (b) (molecule labeled A-grey B-sky blue) molecules are linked by hydrogen bonds and C–H···π interactions on ac plane, (c) molecules are stacking along *b* axis with hydrogen bonds with the closest centroid distance (d_{c-c} = 5.311(5) Å) between the adjacent anthracene rings showed by violet lines. The dotted lines show hydrogen bonds and C–H···π interactions, respectively. Hydrogen atoms not participating in the interactions have been omitted for clarity.

Table 3 C–X···π and N–O···π interactions in these forms

Crystal	Interaction	Distance[a] (Å)	Angle[b] (°)
$\mathbf{I_a}$	C_{15}–$H_{(15A)}$···6 atoms of anthracene	2.860	127.00
$\mathbf{I_b}$	C_4–$H_{(4A)}$···benzene ring	2.950	156.00
	C_{22A}–$H_{(22A)}$···6 atoms of anthracene	2.890	131.00
	C_{4B}–$H_{(4B)}$···benzene ring	2.960	157.00
	C_{22B}–$H_{(22B)}$···6 atoms of anthracene	2.920	130.00
$\mathbf{II_a}$	C_{12}–$H_{(12A)}$···benzene ring	2.710	147.00
	C_{22}–$H_{(22A)}$···6 atoms of pyrene ring	2.870	136.00
	C_{19}–O···6 atoms of pyrene ring	3.900(5)	80.1(4)
$\mathbf{II_b}$	C_{23}–Cl···6 atoms of pyrene ring	3.968	101.82
	C_{23}–Cl···6 atoms of benzene ring	3.678	90.42
$\mathbf{III_a}$	C_{16}–$H_{(16A)}$···benzene ring	2.790	144.00
$\mathbf{III_b}$	$C_{(12A)}$–$H_{(12A)}$···benzene ring	2.760	146.00
	$C_{(12B)}$–$H_{(12B)}$…benzene ring	2.860	149.00
	C_{19}–$O_{(1A)}$···6 atoms of pyrene ring	3.896	83.4(2)
$\mathbf{IV_a}$	C_{19}–$O_{(1)}$···6 atoms of pyrene ring	3.830(4)	74.6(3)
	N–$O_{(3)}$···6 atoms of pyrene ring	3.642(5)	90.5(3)

[a] The distances were measured from hydrogen atom or halogen atom or oxygen atom to the centre of the aromatic ring (for C–X···π, X = H, O, Cl). [b] The angles were measured between C–X–*c* or N–O–*c* (for C–X···π or N–O···π).

chromophores).[28,29] And it can be found that J-type aggregation exists in $\mathbf{II_a}$, $\mathbf{III_b}$, $\mathbf{IV_a}$ (Fig. 3b, 6b and 8b). The closest centroid distance (d_{c-c}) between adjacent anthracene or pyrene rings follow as below (Table 4): 5.431(3) Å, 5.311(5) Å for $\mathbf{I_a}$, $\mathbf{I_b}$ of anthracene system and 5.507(4) Å, 4.818(5) Å, 5.505(4) Å, 5.488(2) Å, 4.672(4) Å, 7.784(0) Å for $\mathbf{II_a}$, $\mathbf{II_b}$, $\mathbf{III_a}$, $\mathbf{III_b}$, $\mathbf{III_c}$, $\mathbf{IV_a}$ of pyrene system. The smallest value of closest centroid distance (d_{c-c}) in these systems is 4.672(4) Å which corresponds to crystal $\mathbf{III_c}$. The interplanar separation ($d_{\pi-\pi}$) and lateral displacement (R) between the mean planes of the pyrene moieties for $\mathbf{III_c}$ are 3.462(3) Å and 3.137 Å respectively, which indicate that weak π–π interactions existing between the neighboring pyrene chromophores. No such interactions exist in all other crystal forms.

As shown in Table 5, the dihedral angles between benzene ring and anthracene ring in $\mathbf{I_b}$ are much larger than that of $\mathbf{I_a}$. The dihedral angles between benzene ring and pyrene ring in $\mathbf{III_a}$ are also larger than any other crystal forms containing pyrene chromophore. This indicates that *cis* configuration exhibits worse molecular coplanarity between aromatic rings than *trans* configuration. This result can also be inferred from the torsion angles data (Table 6 and Scheme 3).

Powder X-ray diffraction analysis

All these crystal forms were determined by powder X-ray diffraction (PXRD) analysis. Remarkably, the PXRD pattern indicates distinct difference for different crystal forms of the same compound (Fig. 9).

Furthermore, PXRD curves coincide well with simulated data calculated from the SXRD data which suggests these forms are in high purity (Fig. 10S, ESI†).

Thermal properties analysis

The thermal behaviors of these crystals were investigated by DSC and TGA. It can be seen from Fig. 10 that both $\mathbf{I_a}$ and $\mathbf{I_b}$ show a endothermic peak at 136 °C and 144 °C, respectively. $\mathbf{II_b}$ exists only one endothermic peak at 161 °C. Both $\mathbf{II_a}$ and $\mathbf{II_c}$ own two endothermic peaks at 144 °C, 156 °C and 118 °C, 131 °C. $\mathbf{III_a}$, $\mathbf{III_b}$, $\mathbf{III_c}$ and $\mathbf{III_d}$ exhibit one endothermic peak at 120 °C, 160 °C, 165 °C and 156 °C, respectively. Both $\mathbf{IV_a}$ and $\mathbf{IV_b}$ show an endothermic peak with pretty similar temperatures of 215.8 °C and 215.5 °C.

Optical–physical properties

$\mathbf{I_a}$ and $\mathbf{I_b}$ show similar absorption band in 300–400 nm in acetonitrile which are attributed to anthracene chromophore. All forms with pyrene ring have similar absorption band in 300–450 nm in acetonitrile which are attributed to pyrene chromophore (Fig. 11S, ESI†). As shown in Fig. 11, absorption bands of all crystal forms have red shifted relative to their solution. Furthermore, $\mathbf{I_a}$ shows a red shifted absorption edge than that of $\mathbf{I_b}$ which can be ascribed to *trans* configuration of $\mathbf{I_a}$. $\mathbf{II_a}$ has the largest absorption edge wavelength in three crystal forms of chalcone **II**. $\mathbf{II_c}$ owns the smallest absorption wavelength. Likewise, $\mathbf{III_b}$ shows the largest absorption edge wavelength in four crystal forms of chalcone **III**. In addition, $\mathbf{IV_b}$ shows a red shift in comparison with $\mathbf{IV_a}$. All these results are positively

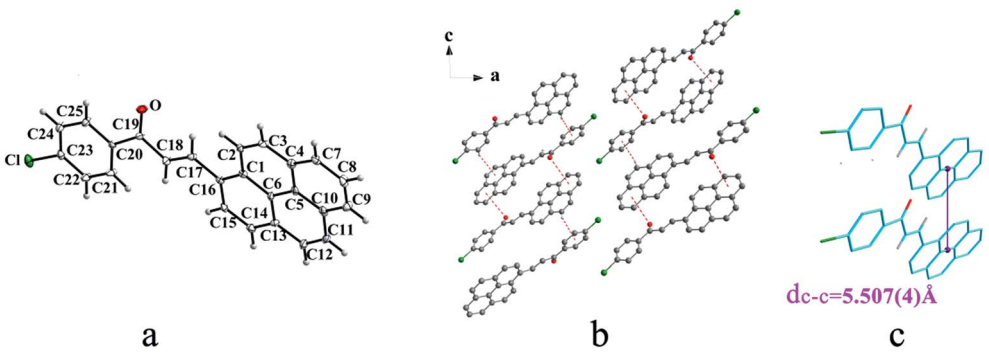

Fig. 3 Structure of form $\mathbf{II_a}$: (a) *trans* configuration, (b) molecules are linked by C–O···π and C–H···π interactions on ac plane, (c) the violet line represents the closest centroid distance (d_{c-c} = 5.507(4) Å) between the adjacent anthracene rings. The dotted lines show hydrogen bonds and C–H···π interactions, respectively. Hydrogen atoms not participating in the interactions have been omitted for clarity.

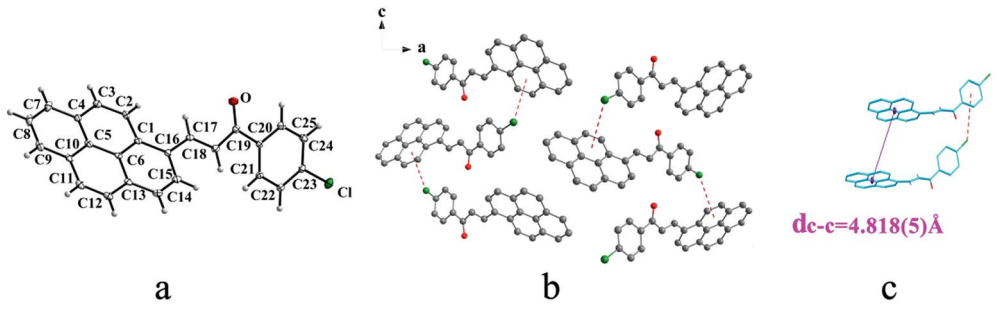

Fig. 4 Structure of form II_b: (a) *trans* configuration, (b) molecules are linked by C–Cl···π interactions on ac plane, (c) molecules are stacking along *c* axis with C–Cl···π interactions. The violet line represents the closest centroid distance (d_{c-c} = 4.818(5) Å) between the adjacent anthracene rings. The dotted lines show C–Cl···π interactions, respectively. Hydrogen atoms not participating in the interactions have been omitted for clarity.

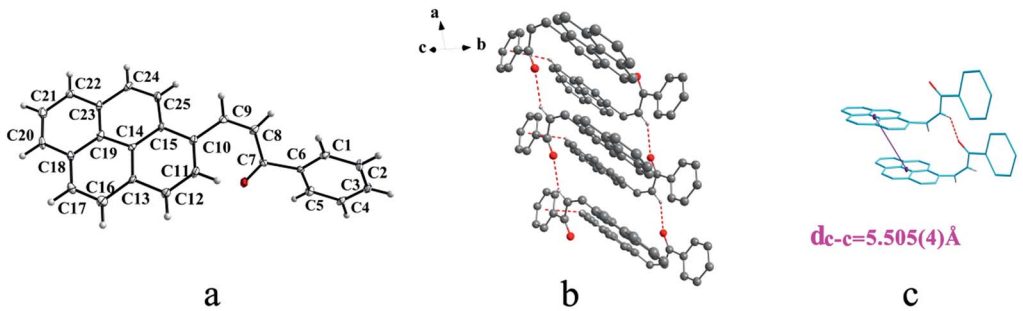

Fig. 5 Structure of form III_a: (a) *cis* configuration, (b) molecules are linked by C–H···π and C–H···O interactions on *ab* plane, (c) the violet line represents the closest centroid distance (d_{c-c} = 5.505(4) Å) between the adjacent anthracene rings. The dotted lines show C–H···π and C–H···O interactions, respectively. Hydrogen atoms not participating in the interactions have been omitted for clarity.

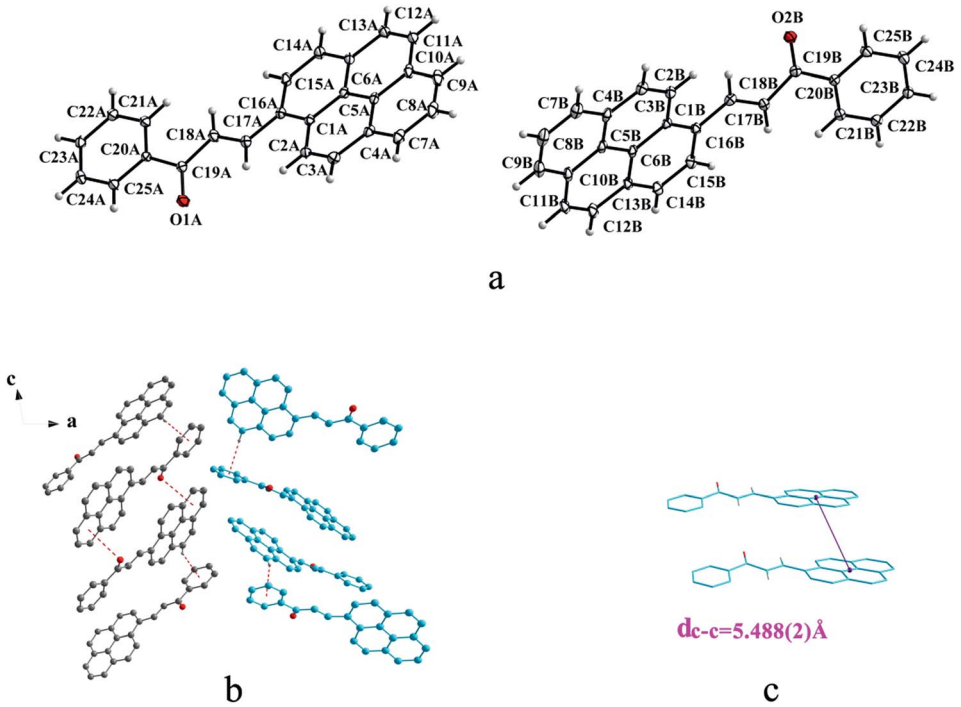

Fig. 6 Structure of form III_b: (a) *trans* configuration, (b) (type A-grey type B-sky blue) molecules are linked by C–H···π and C–O···π interactions on ac plane, (c) the violet line represents the closest centroid distance (d_{c-c} = 5.488(2) Å) between the adjacent anthracene rings. The dotted lines show C–H···π and C–O···π interactions, respectively. Hydrogen atoms not participating in the interactions have been omitted for clarity.

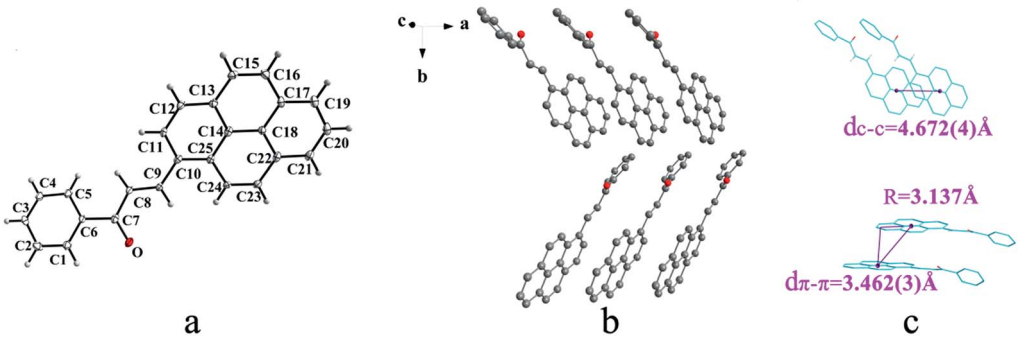

Fig. 7 Structure of form III_c: (a) *trans* configuration, (b) molecules are stacking on *ab* plane with slipped face-to-face π···π interaction, (c) the d_{c-c}, $d_{\pi-\pi}$ and *R* are 4.672(4) Å, 3.462(3) Å and 3.137 Å, respectively. Hydrogen atoms not participating in the interactions have been omitted for clarity.

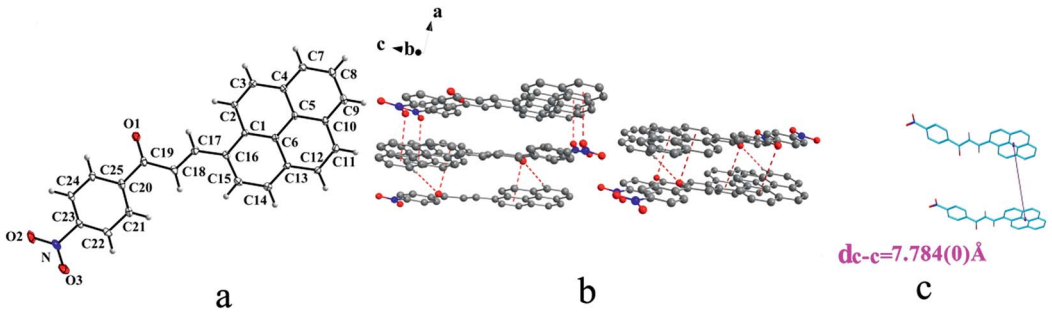

Fig. 8 Structure of form IV_a: (a) *trans* configuration, (b) molecules are linked by C–H···O, C–O···π and N–O···π interactions on ac plane, (c) the violet line represents the closest centroid distance (d_{c-c} = 7.847(0) Å) between the adjacent anthracene rings. The dotted lines show C–H···O, C–O···π and N–O···π interactions, respectively. Hydrogen atoms not participating in the interactions have been omitted for clarity.

correlated with molecular coplanarity in these crystals discussed following.

$\mathbf{I_a}$ and $\mathbf{I_b}$ show similar emission band in 450–500 nm in cyclohexane (Fig. 12S, ESI†) which are attributed to anthracene chromophore. All forms with pyrene chromophore have similar emission bands in *trans* configuration were found to have fluorescence and have red shifted in comparison with their solutions.

In solid states, only those with *trans* configuration were found to have fluorescence and have red shifted in comparison with their solutions. $\mathbf{I_a}$ has a emission peak at 548 nm which shows a red shifted in contrast with the emission spectra of anthracene crystal.

Similarly, emission spectra of crystals with pyrene chromophore exhibit a red shift in comparison with pyrene which shows characteristic peak at 470 nm. All these can be explained by larger conjugation system than pyrene and overwhelming intermolecular interactions in these crystals. As shown in Fig. 12, forms $\mathbf{II_a}$, $\mathbf{III_b}$, $\mathbf{IV_a}$ have longer emission peaks (600–650 nm) relative to that of forms $\mathbf{I_a}$, $\mathbf{II_b}$, $\mathbf{III_c}$, $\mathbf{III_d}$ (570–500 nm). These results can be explained by molecular coplanarity in these crystals.

Table 4 The closest centroid distance d_{c-c} between anthracene or pyrene rings

Crystal	d_{c-c} (Å)
$\mathbf{I_a}$	5.431(3)
$\mathbf{I_b}$	5.311(5)
$\mathbf{II_a}$	5.507(4)
$\mathbf{II_b}$	4.818(5)
$\mathbf{III_a}$	5.505(4)
$\mathbf{III_b}$	5.488(2)
$\mathbf{III_c}$	4.672(4)
$\mathbf{IV_a}$	7.784(0)

Table 5 The dihedral angles between the benzene ring and anthracene ring/pyrene ring

Crystal	Angles (°)
$\mathbf{I_a}$	35.0(2)
$\mathbf{I_b}$	67.8(4)/68.1(3)[a]
$\mathbf{II_a}$	7.8(2)
$\mathbf{II_b}$	48.3(3)
$\mathbf{III_a}$	72.0(2)
$\mathbf{III_b}$	9.02(13)/15.62(13)[a]
$\mathbf{III_c}$	39.0(3)
$\mathbf{IV_a}$	3.32(16)

[a] The first one is the dihedral angle of molecule A in asymmetry unit and the second one is the dihedral angle of molecule B.

Table 6 Torsion angles of crystal forms

Compound	Molecules	C1–C2–C3–C4/°	C3–C4–C5–O/°	C4–C5–C6–C7/°
I	$\mathbf{I_a}$	−52.3(9)	−0.7(8)	23.8(8)
	A of $\mathbf{I_b}$	−58.0(1)	−41.9(1)	−12.4(1)
	B of $\mathbf{I_b}$	54.6(1)	40.0(1)	12.2(4)
II	$\mathbf{II_a}$	11.9(1)	4.9(1)	−5.4(9)
	$\mathbf{II_b}$	20.0(1)	13.6(1)	13.4(1)
III	$\mathbf{III_a}$	43.6(8)	18.9(8)	29.4(7)
	A of $\mathbf{III_b}$	−11.1(6)	−2.5(6)	8.8(5)
	B of $\mathbf{III_b}$	−15.2(6)	−6.5(6)	12.0(5)
	$\mathbf{III_c}$	9.4(1)	10.5(1)	22.4(1)
IV	$\mathbf{IV_a}$	7.2(7)	−0.4(7)	−7.5(6)

Crystals of forms $\mathbf{II_a}$, $\mathbf{III_b}$, $\mathbf{IV_a}$ show the least torsion extent and smallest dihedral angles among these forms so that they own the largest emission peak wavelengths which are consistent with their red fluorescence in microscopy images in Fig. 13. Besides, forms $\mathbf{II_c}$ and $\mathbf{III_d}$ may own the similar molecules planarity to those of $\mathbf{I_a}$ and $\mathbf{III_c}$ by comparing their fluorescence even no SCXRD data.

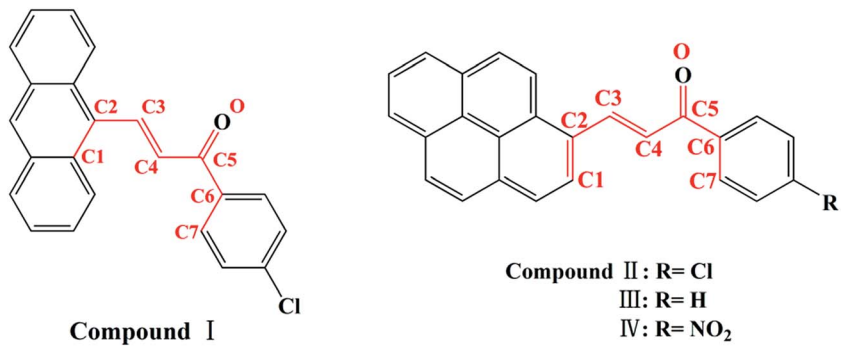

Scheme 3 Chemical structure with torsion angles labeled.

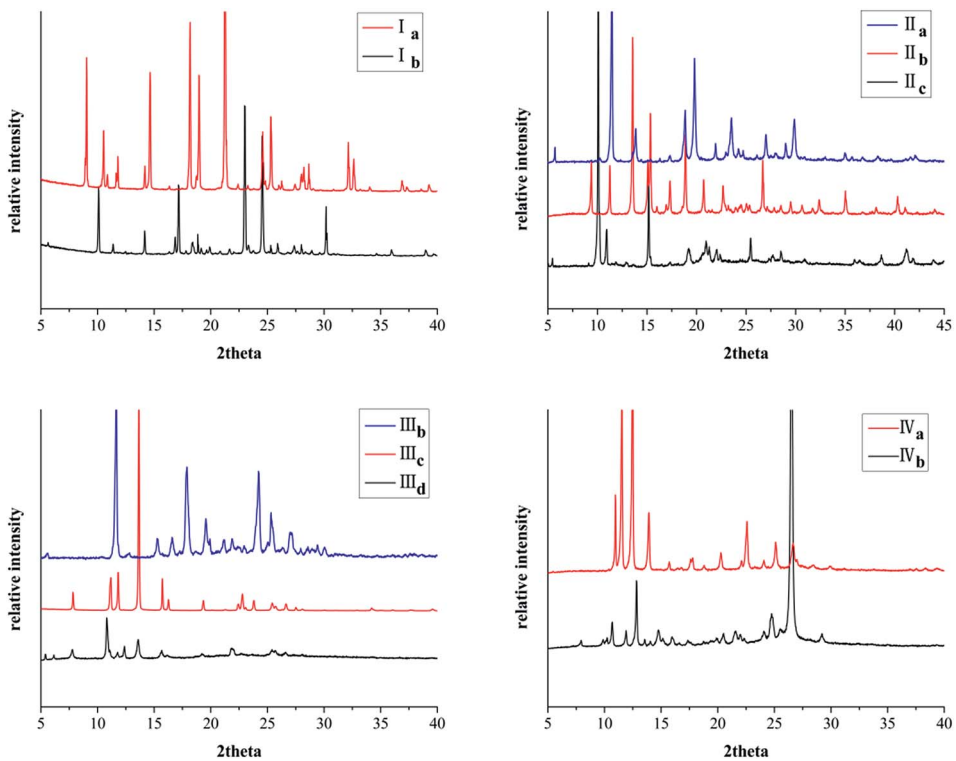

Fig. 9 PXRD patterns of crystals.

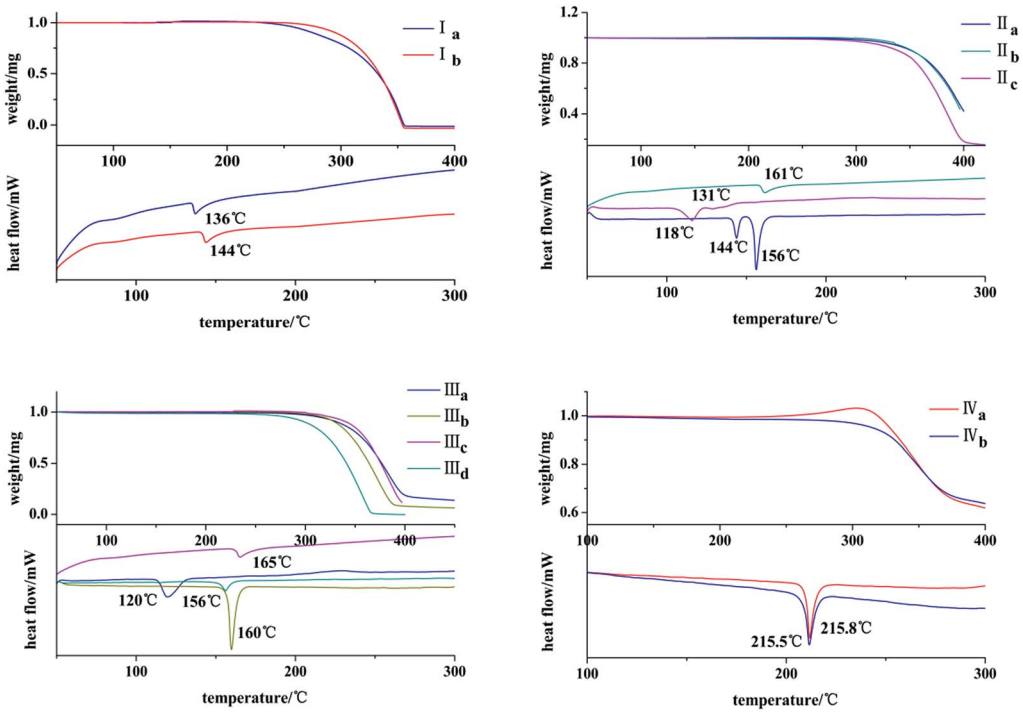

Fig. 10 TGA/DSC profiles of crystals.

In addition, it has been found that J-aggregates formed in the polymorphs. Researches on the luminescence properties have shown that J-aggregates are highly emissive.[19] **II$_a$** show a red shifted emission band in contrast with the emission spectra in solution which suggests the J-aggregates formation in its solid state(Fig. 12S, ESI† and Fig. 12). And **II$_a$** has the larger emission wavelength than **II$_b$** for no J-aggregates form in **II$_b$** (Fig. 4 and 12). Likewise, molecules in **III$_b$** also form J-

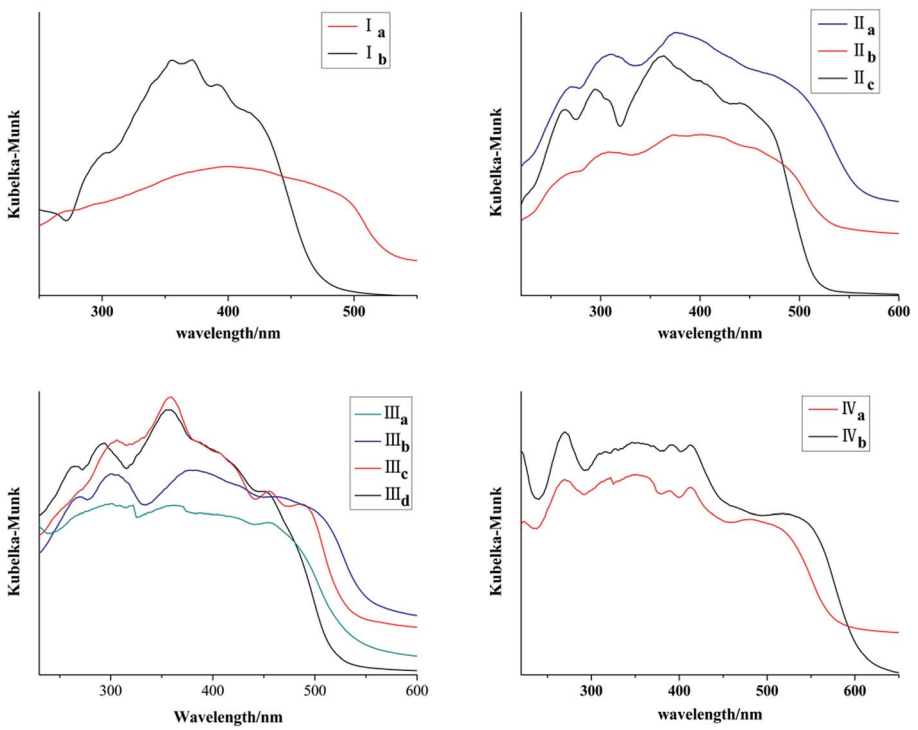

Fig. 11 Solid-state adsorption spectra of crystals.

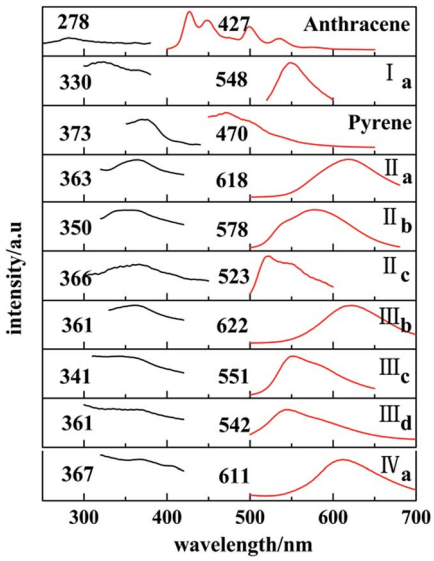

Fig. 12 Solid-state excitation spectra (black) and fluorescence emission spectra (red).

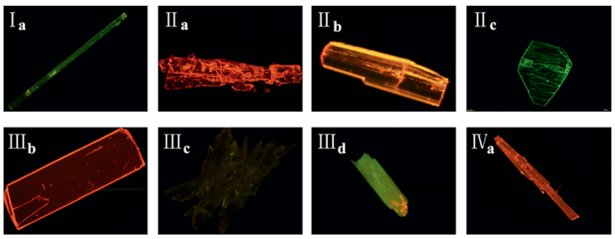

Fig. 13 Fluorescence microscopy images of eight crystals under UV light (λ_{ex} = 365 nm).

aggregates so that **III$_b$** shows a red shift in solid state emission spectra in comparison with its emission bands in solution. As for **III$_c$**, π···π interaction exists in its crystal structure which may induce the excimer formation among pyrene rings. And excimer formation leads to the suppression of fluorescence[30] so that **III$_c$** exhibit a blue shifted emission band in contrast with **III$_b$**. In Fig. 8 and 12, molecular aggregation of J-type exists in **IV$_a$** which leads to a red shift in its solid state emission spectra.

FT-IR spectroscopy

As for FT-IR spectra (Fig. 13S, ESI†), there are two strong vibrational peaks in 1670–1520 cm^{-1} being magnified in the figure. These two peaks should be separately assigned to carbonyl group with high frequency and ethenyl group in all forms.

Hirshfeld surface calculation

The Hirshfeld surface calculation has been used for all crystals. As shown in Fig. 14 and Table 7, the analysis of forms **I$_a$** and **I$_b$** was carried out in terms of d_{norm} surface and fingerprint plots. In addition, the calculation of other forms is listed in ESI (Fig. 14S, ESI†).

Hirshfeld surface mapped with d_{norm} takes size of atoms into consideration thus comes out normalized contact distance d_{norm} which is calculated from d_e (nearest external distance), d_i (nearest internal distance) and the van der Waals (vdW) radii of the two atoms to the surface.[31] The fingerprint plot derives from Hirshfeld surface that represented by a coordinate (d_i, d_e). The colors indicate the number of points with a given fingerprint

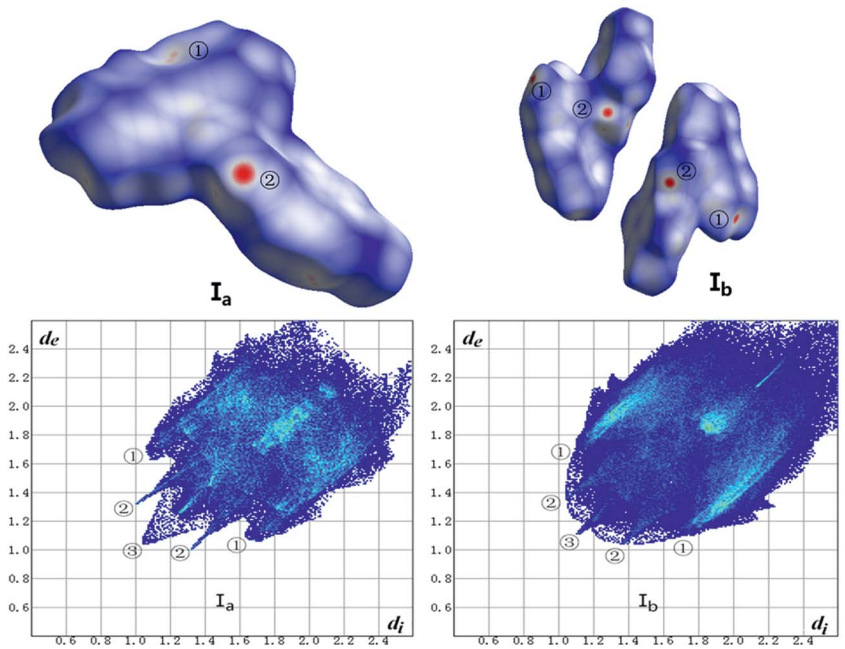

Fig. 14 Hirshfeld surface mapped with d_{norm} (top) and fingerprint plots (bottom) of I$_b$ and I$_b$. Hirshfeld surface colored by d_{norm}, showing as a red-white-blue scheme as d_{norm} increase.

Table 7 Contributions of individual intermolecular interactions to the Hirshfeld surface of I_a and I_b

Polymorph	C–H	O–H	H–H	C–C
$\mathbf{I_a}$	33.8%	7.6%	36.9%	6.0%
$\mathbf{I_b}$	35.7%	9.3%	35.6%	3.6%

plot coordinate ranging from blue (relatively few points) through green (moderate fraction) to red (many points).

As shown in Fig. 14, the red hotpots marked ② on the d_{norm} surface of $\mathbf{I_a}$ and $\mathbf{I_b}$ correspond to strong C–H···O hydrogen bonds. And d_{norm} surface of $\mathbf{I_b}$ shows another two red hotpots labeled ① respectively on the surface of two molecules that can be assigned to C–H···π interactions while the same interactions of $\mathbf{I_a}$ just exhibit light red spot on the upper right of the surface which indicates weaker C–H···π contacts in crystal structure of $\mathbf{I_a}$ than $\mathbf{I_b}$.

The two wings marked ① in the fingerprint plots represent C–H···π. The contact C–H···π contributes 33.8% and 35.6% of the total Hirshfeld surface respectively for $\mathbf{I_a}$ and $\mathbf{I_b}$. The little spikes marked ② can be assigned to C–H···O hydrogen bonds which separately contributes 7.6% and 9.2% to the whole Hirshfeld surface of $\mathbf{I_a}$ and $\mathbf{I_b}$. The slightly larger contribution of C–H···O hydrogen bonds in $\mathbf{I_b}$ make a contribution to its higher melting point than $\mathbf{I_a}$ which coincides with results of thermal analysis. Besides, the H···H contacts, as indicated by the blue region marked ③ diffuses around the diagonal, making a significant contribution towards the solid-state stabilization of the two polymorphs. They are 36.9% and 35.7% for $\mathbf{I_a}$ and $\mathbf{I_b}$. The center area of the plots where $d_e + d_i \approx 3.6$ Å corresponds to π···π (C···C) interactions which contributes only 6.0% and 3.6% for $\mathbf{I_a}$ and $\mathbf{I_b}$. To some extent, the worse planarity of $\mathbf{I_b}$ than $\mathbf{I_a}$ may give a explanation to the different contribution of π···π (C···C) contacts between $\mathbf{I_a}$ and $\mathbf{I_b}$.

Conclusion

In summary, we demonstrated eight chalcone crystal structures in detail. It is evident that the compound of chalcone can crystallize in different configurations or conformations in different solvent systems. Crystals with *trans* configuration are fluorescent while those with *cis* configuration are not. Furthermore, forms $\mathbf{II_a}$, $\mathbf{III_b}$, $\mathbf{IV_a}$ exist larger red-shifted emissions than forms $\mathbf{I_a}$, $\mathbf{II_b}$, $\mathbf{III_c}$ which can be attributed to better molecular coplanarity and J-aggregates formation in $\mathbf{II_a}$, $\mathbf{III_b}$, $\mathbf{IV_a}$. It implies that solid-state fluorescence of chalcone crystals can be tuned by crystal engineering. And the strategy of tuning molecular coplanarity and J-aggregates formation through polymorphism may provide useful information into organic light-emitting materials.

Acknowledgements

This project is supported by the National Basic Research Program of China (Grant 2011CB302004) and the Priority Academic Program Development of Jiangsu Higher Education Institutions.

Notes and references

1 R. J. Davey, *Chem. Commun.*, 2003, **13**, 1463–1467.
2 J. Bernstein, *Polymorphism in Molecular Crystals*, Oxford University Press, New York, 2002.
3 S. S. Kumar and A. Nangia, *Cryst. Growth Des.*, 2014, **14**(4), 1865–1881.
4 L. Q. Yang, Q. X. Yin, B. H. Hou, Y. Bao, J. K. Wang and H. X. Hao, *Ind. Eng. Chem. Res.*, 2013, **52**(7), 2477–2485.
5 P. Singh, A. Anandb and V. Kumarc, *Eur. J. Med. Chem.*, 2014, **85**, 758–777.
6 U. J. Griesser, R. K. R. Jetti, M. F. Haddow, T. Brehmer, D. C. Apperley, A. King and R. K. Harris, *Cryst. Growth Des.*, 2008, **8**(1), 44–56.
7 G. Klebe, F. Graser and E. Hadicke, *Acta Crystallogr., Sect. B: Struct. Sci.*, 1989, **45**, 69–77.
8 H. G. Gallagher and J. N. Sherwood, *J. Chem. Soc., Faraday Trans.*, 1996, **92**(12), 2107–2116.
9 S. J. Yoon and S. Y. Park, *J. Mater. Chem.*, 2011, **21**, 8338–8346.
10 S. H. Lapidus, A. Naik, A. Wixtrom, N. E. Massa, V. Ta Phuoc, L. del Campo, S. Lebegue, J. G. Angyan, T. Abdel-Fattah and S. Pagola, *Cryst. Growth Des.*, 2014, **14**, 91–100.
11 R. A. Esteves de Castro, J. Canotilho, R. M. Barbosa, M. R. Silva, A. M. Beja, J. A. Paixao and J. S. Redinha, *Cryst. Growth Des.*, 2007, **7**(3), 496–500.
12 T. M. R. Maria, R. A. E. Castro, S. S. Bebiano, M. R. Silva, A. M. Beja, J. Canotilho and M. E. S. Eusebio, *Cryst. Growth Des.*, 2010, **10**, 1194–1200.
13 P. S. Pereira Silva, R. A. E. Castro, E. Melro, M. R. Silva, T. M. R. Maria, J. Canotilho and M. E. S. Eusebio, *J. Therm. Anal. Calorim.*, 2015, **120**(1), 667–677.
14 G. Q. Zhang, J. W. Lu, M. Sabat and C. L. Fraser, *J. Am. Chem. Soc.*, 2010, **132**, 2160–2162.
15 S. Kervyn, O. Fenwick, F. Di Stasio, Y. S. Shin, J. Wouters, G. Accorsi, S. Osella, D. Beljonne, F. Cacialli and D. Bonifazi, *Chem.–Eur. J.*, 2013, **19**, 7771–7779.
16 S. P. Anthony, *Chem.–Asian J.*, 2012, **7**(3), 374–379.
17 R. M. Zhang, M. L. Wang, H. Sun, A. Khan, R. Usman, S. Z. Wang, X. T. Gu, J. Wang and C. X. Chun, *New J. Chem.*, 2016, **44**, 6441–6450.
18 F. Wurthner, T. E. Kaiser and C. R. Saha-Moller, *Angew. Chem., Int. Ed.*, 2011, **13**, 3376–3410.
19 Y. H. Deng, W. Yuan, Z. Jia and G. Jiu, *J. Phys. Chem. B*, 2014, **118**, 14536–14545.
20 A. M. Asiri and S. A. Khan, *Mater. Lett.*, 2011, **65**, 1749–1752.
21 P. S. Patil, S. R. Maidur, S. V. Rao and S. M. Dharmaprakash, *Opt. Laser Technol.*, 2016, **81**, 70–76.
22 Z. K. Si, Q. Zhang, M. Z. Xue, Q. R. Sheng and Y. G. Liu, *Res. Chem. Intermed.*, 2011, **37**(6), 635–646.
23 A. M. Asiri and S. A. Khan, *J. Heterocycl. Chem.*, 2012, **49**(6), 1434–1438.
24 H. Singh, J. Sindhu and J. M. Khurana, *J. Lumin.*, 2015, **158**, 340–350.

25 R. Nithya, N. Santhanamoorthi, P. Kolandaivel and K. Senthilkumar, *J. Phys. Chem. A*, 2011, **115**, 6594–6602.
26 Y. X. Li, H. B. Zhou, J. L. Miao, G. X. Xun, G. B. Li, Y. Nie, C. L. Chen, Z. Chen and X. T. Tao, *CrystEngComm*, 2012, **14**, 8286–8291.
27 Y. B. Wang, Z. L. Wang, T. L. Liang, H. B. Fu and J. N Yao, *Acta Crystallogr., Sect. E: Struct. Rep. Online*, 2008, **64**, o630.
28 E. G. McRae and M. Kasha, *J. Chem. Phys.*, 1958, **28**, 721–722.
29 M. Kasha, R. Rawls and M. A. El-Bayoumi, *Pure Appl. Chem.*, 1965, **11**, 371–392.
30 J. N. Moorthy, P. Venkatakrishnan, D. F. Huang and T. J. Chow, *Org. Lett.*, 2007, **9**(25), 5215–5218.
31 M. A. Spackman and D. Jayatilaka, *CrystEngComm*, 2009, **11**, 19–32.